

niques were used to fabricate mesa structures, in which single dot molecules can be isolated due to the small lateral sizes (~ 100 nm) (33). The luminescence of single QD molecules, from which the evolution of the molecule states with decreasing dot separation (from top to bottom) is seen, is shown in Fig. 3A. The spectra were recorded at low excitation powers to avoid emission from multiexciton complexes. The temperature was ~ 60 K so that not only ground state exciton emission, but also emission from excited exciton states is observed due to thermal excitation. In each case, symmetric single QD molecules were selected whose ground state emission is located at the center of the emission band of the corresponding arrays. The top trace in Fig. 3A shows the emission of a single QD which serves as reference for the emission from the QD molecules.

For a large dot separation $d = 16$ nm in a molecule (34), two emission lines are observed in the s-shell with a splitting varying from 0 to 4 meV. For this distance and temperature, interaction with acoustical phonons prevents coherent tunneling, and we expect that the recombination takes place from either state $|0,0\rangle$ or $|1,1\rangle$ in individual QDs. The small splitting arises from dot inhomogeneities. For a dot separation $d = 8$ nm, the s-shell emission splits into the entangled exciton states $|a'\rangle$ and $|b'\rangle$ (eigenstates of the electron-hole Hamiltonian). The energy splitting between them is about 10 meV. In addition, a further emission line denoted by $|\alpha\rangle$ appears on the high energy side. The energies of all these features depend systematically on d : Reduction of the QD separation moves the emission line $|a'\rangle$ strongly to lower energies, while the energy of the peak $|b'\rangle$ is almost constant leading to an increase of their splitting to more than 25 meV. This behavior is suggestive of the energy level splitting due to the dot coupling. Hence we ascribe the two emission lines as originating from the entangled states of the s-shell exciton. The line $|\alpha\rangle$, on the other hand, moves to lower energies with decreasing d and can be assigned to the lowest entangled state from the p-shell.

The transition energies (summarized in Fig. 3B) show the dependence of exciton transition energies in the QD molecules in Fig. 3A versus wetting layer separation d . The observed behavior is in qualitative agreement with that expected from the model calculations in Fig. 2. Most importantly, the splitting between the optically active entangled exciton states of the s-shell is more than 30 meV when the barrier width becomes smaller than 5 nm. Despite the statistical variations, the observed trends, in particular for the energy splitting among the levels, are typical for the studied QD molecules.

References and Notes

1. C. H. Bennett, *Phys. Today* **48** (no. 10), 24 (1995).
 2. D. P. DiVincenzo, *Science* **270**, 255 (1995).
 3. A. Steane, *Rep. Prog. Phys.* **61**, 117 (1998).

4. G. Mahler, in *Information: New Questions to a Multidisciplinary Concept*, K. S. Kornwachs, K. Jacoby, Eds. (Akademie Verlag, Berlin, 1999), pp. 103–118.
 5. A. Barenco, D. Deutsch, A. Ekert, R. Jozsa, *Phys. Rev. Lett.* **74**, 4083 (1995).
 6. J. A. Brum, P. Hawrylak, *Superlattices Microstruct.* **22**, 431 (1997).
 7. D. Loss, D. P. DiVincenzo, *Phys. Rev. A* **57**, 120 (1998).
 8. P. Zanardi, F. Rossi, *Phys. Rev. Lett.* **81**, 4752 (1998).
 9. C. A. Sackett et al., *Nature* **404**, 256 (2000).
 10. I. L. Chuang, L. M. K. Vandersypen, X. Zhou, D. W. Leung, S. Lloyd, *Nature* **393**, 143 (1998).
 11. P. Hawrylak, S. Fafard, Z. R. Wasilewski, *Condens. Matter News* **7**, 16 (1999).
 12. J. J. Palacios, P. Hawrylak, *Phys. Rev. B* **51**, 1769 (1995).
 13. R. H. Blick, D. Pfannkuche, R. J. Haug, K. von Klitzing, K. Eberl, *Phys. Rev. Lett.* **80**, 4032 (1998).
 14. T. Fujisawa et al., *Science* **282**, 932 (1998).
 15. L. Kouwenhoven, *Science* **268**, 1440 (1995).
 16. G. Schedelbeck, W. Wegscheider, M. Bichler, G. Abstreiter, *Science* **278**, 1792 (1997).
 17. D. G. Austing, T. Honda, K. Muraki, Y. Tokura, S. Tarucha, *Physica B* **249**, 206 (1998).
 18. R. J. Luyken et al., *Nanotechnology* **10**, 14 (1999).
 19. Y. Tokura, D. G. Austing, S. Tarucha, *J. Phys. Condens. Matter* **11**, 6023 (1999).
 20. C. Pryor, *Phys. Rev. Lett.* **80**, 3579 (1998).
 21. L. R. C. Fonseca, J. L. Jimenez, J. P. Leburton, *Phys. Rev. B* **58**, 9955 (1998).
 22. L. Goldstein, F. Glas, J. Y. Marzin, M. N. Charasse, G. LeRoux, *Appl. Phys. Lett.* **47**, 1099 (1985).
 23. P. R. Berger, K. Chang, P. Bhattacharya, J. Singh, K. K. Bajaj, *Appl. Phys. Lett.* **53**, 684 (1988).
 24. Q. Xie, A. Madhukar, P. Chen, N. P. Kobayashi, *Phys. Rev. Lett.* **75**, 2542 (1995).
 25. G. S. Solomon, J. A. Trezza, A. F. Marshall, J. J. S. Harris, *Phys. Rev. Lett.* **76**, 952 (1996).
 26. S. Rouvimov et al., *J. Electron. Mater.* **27**, 427 (1998).
 27. S. Fafard, M. Spanner, J. P. McCaffrey, Z. Wasilewski, *Appl. Phys. Lett.* **76**, 2707 (2000).
 28. S. Fafard et al., *Phys. Rev. B* **59**, 15368 (1999).
 29. Z. R. Wasilewski, S. Fafard, J. P. McCaffrey, *J. Cryst. Growth* **201**, 1131 (1999).
 30. J. P. McCaffrey et al., *J. Appl. Phys.* **88**, 2272 (2000).
 31. M. Korkusinski, P. Hawrylak, in preparation.
 32. A. Wojs, P. Hawrylak, S. Fafard, L. Jacak, *Phys. Rev. B* **54**, 5604 (1996).
 33. M. Bayer, O. Stern, P. Hawrylak, S. Fafard, A. Forchel, *Nature* **405**, 923 (2000).
 34. M. Bayer et al., data not shown.
 35. This work has been carried out under the Canadian European Research Initiative on Nanostructures supported by the European Commission (IST-FET program); by the Institute for Microstructural Sciences, Canadian National Research Council (IMS NRC); and by the Canadian Natural Sciences and Engineering Research Council. The Würzburg group acknowledges support by the Deutsche Forschungsgemeinschaft, the U.S. Defense Advanced Research Projects Agency, and the State of Bavaria. M.K. thanks the IMS NRC for financial support; P.H. thanks the Alexander von Humboldt Foundation for support.

21 July 2000; accepted 4 December 2000

A Lost-Wax Approach to Monodisperse Colloids and Their Crystals

Peng Jiang, Jane F. Bertone, Vicki L. Colvin*

We report a nanoscale “lost-wax” method for forming colloids with size distributions around 5% and their corresponding colloidal crystals. Macroporous polymer templates are first prepared from a silica colloidal crystal. We then use the uniform and interconnected voids of the porous polymer to generate a wide variety of highly monodisperse inorganic, polymeric, and metallic solid and core-shell colloids, as well as hollow colloids with controllable shell thickness, as colloidal crystals. We can also uniformly deform the polymer template to alter colloidal shape and demonstrate the formation of elliptical particles with precisely controlled aspect ratios.

Monodisperse colloids have uniform physical and chemical properties that are useful for the quantitative evaluation of the optical, magnetic, electrokinetic, or adsorptive behavior of colloidal matter. In addition, highly uniform colloids offer superior properties for commercial applications ranging from magnetic recording to optical pigments (1). When sedimented, colloids with size distributions less than 5% can form three-dimensional (3D) periodic colloidal crystals. Existing strategies for preparing monodisperse colloids and nanoparticles generally manipulate

the chemistry of colloid formation (1, 2). Only silica and some polymer colloids can be routinely prepared with the narrow size distributions required for forming monolithic high-quality colloidal crystals (3). Unfortunately, these colloids do not exhibit the optical, nonlinear optical, or electro-optical functionality of other materials. In addition, although several methods have been developed to make colloidal crystals from silica and polymer colloids (4), colloidal crystallization is difficult for other denser colloids.

We report a physical rather than chemical strategy for forming virtually any colloid with size distributions of 5%. Rather than developing separate chemical methods for different materials, an alternative approach is to use high-quality colloidal crystals to create templates for the formation of a second gen-

Department of Chemistry, Center for Nanoscale Science and Technology, Rice University, Houston, TX 77005, USA.

*To whom correspondence should be addressed. E-mail: colvin@rice.edu

eration of colloidal particles. This approach is similar to the lost-wax method used to create molds for casting sculptures (5). Examples of

such two-step replication processes have been reported. Masuda and colleagues (6) replicated porous glass arrays in TiO_2 . Mallouk and col-

leagues (7) used polymer replicas to replicate silica colloids and also showed that polymer replicas could be shrunk to change the periodicity of the open interconnected mesoporous arrays. In this work, we rely on the uniform and periodic voids of macroporous polymers to contain colloidal growth. A key feature of our macroporous polymers is that they are ordered over large distances (~ 1 cm) and are highly uniform because of the assembly method used to form them. Such long-range order and perfection is essential, as it permits uniform particle formation and fixes the spatial relation of the growing colloids. In addition, this intermediate template provides us with extensive control over particle formation, and diverse colloid shapes and architectures can be formed directly in a dense and crystalline format.

Our method involves two distinct steps: the formation of a macroporous template of a silica colloidal crystal, followed by the growth of new colloids within the voids of the porous polymer (Fig. 1). First, silica colloidal single crystals are formed through a convective assembly method (Fig. 1A) (8). Next, these thin-film arrays are used as templates to generate macroporous polymers containing spherical and ordered voids (Fig. 1B) (9). A key feature of these macroporous polymers is the interconnectedness of their pores; scanning electron microscopy (SEM) (Fig. 1B, inset) shows that each void is connected to its neighbors through smaller windows whose mean dimension can be precisely controlled through the viscosity of the starting monomer (9). Such microstructure allows these macroporous polymers to be filled with different liquid precursor solutions in a second templating process. Further chemical or photochemical reactions then solidify the precursors and fill the cavities (Fig. 1, C and D). The host macroporous polymer can be removed by dissolution in an appropriate solvent, or by heating, leaving behind an array of colloids that retain the initial silica template geometry (Fig. 1, E and F). Although in principle this method could be used with any inverse opal material, polymers are the ideal hosts because they provide for enormous variation in colloidal architecture and shape.

The compatibility of porous polymers with many solvents and chemicals also allows these materials to form a diverse range of colloidal materials within their pores, including ceramic, polymer, semiconductor, and metal nanospheres. For ceramic colloids, the highly iridescent macroporous polystyrene films are first immersed in an alcoholic solution of metal alkoxide; once removed, the alkoxides, which adhere to the inner polymer surfaces, condense as they react with the moisture in air, forming hollow spherical shells. Because the colloids are formed through successive deposition of thin layers

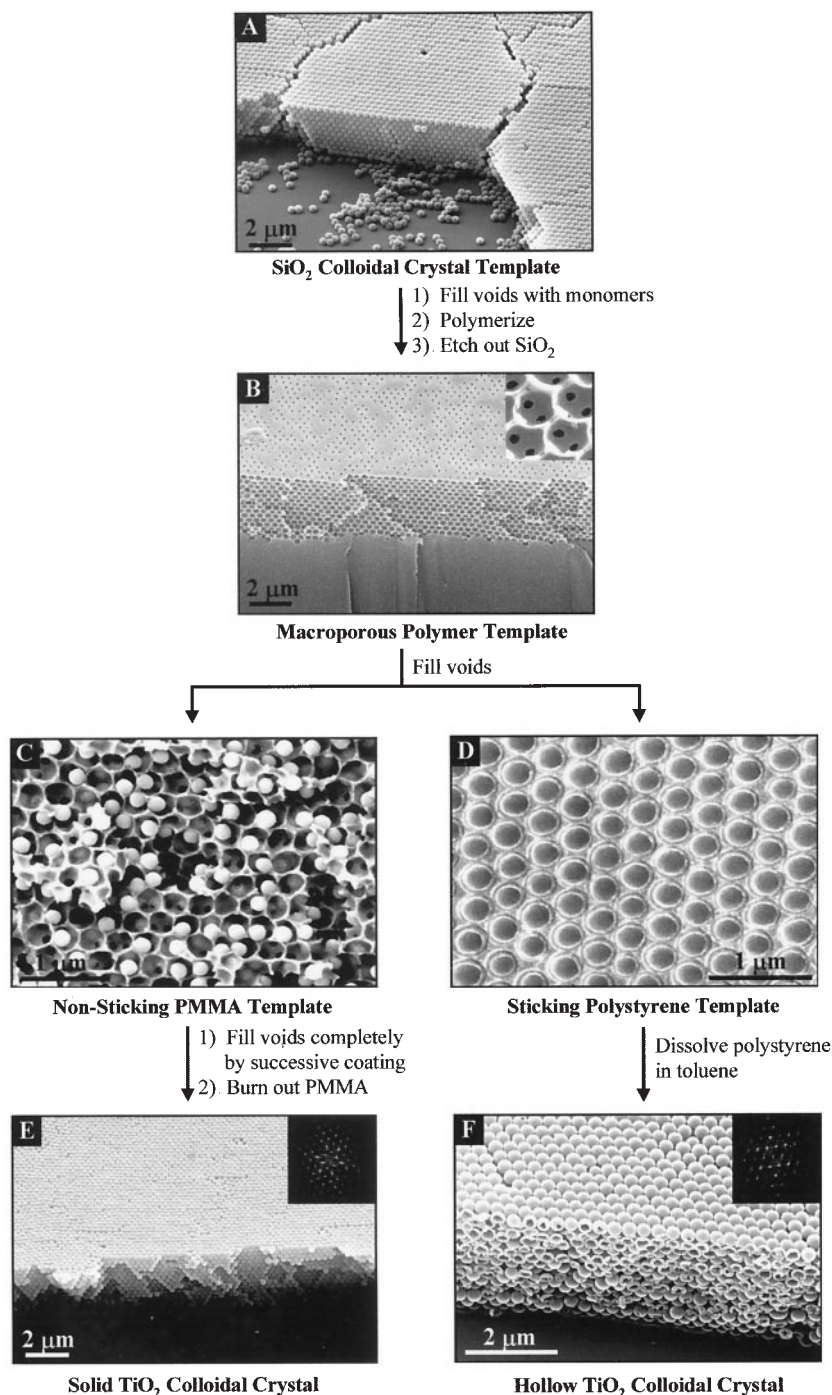


Fig. 1. SEM images at all stages of the templating process. (A) A SiO_2 colloidal crystal template. (B) A macroporous polymer replicated from the crystal shown in (A). The inset shows a higher magnification image of the interconnecting pores between the voids. (C) TiO_2 solid colloids (178 ± 9.8 nm) pull away from the PMMA template (coated twice). (D) TiO_2 hollow colloids (shell thickness 37.9 ± 4.5 nm) adhere strongly to the polystyrene template surface (coated nine times). (E) A solid titania colloidal replica (coated seven times) obtained by burning out the PMMA template with a propane torch. The observed incomplete filling of the voids is reasonable considering the use of diluted metal alkoxides and the large shrinkage (20 to 30%) of alkoxide hydrolysis condensation to form ceramics. A similar reduction in ceramic particle size was observed in a single-step emulsion template method (30). (F) A hollow titania colloidal crystal replica (coated nine times) obtained by dissolving the polystyrene template in toluene. The insets in (E) and (F) show Fourier transforms of $40 \mu\text{m} \times 40 \mu\text{m}$ regions in the (111) plane.

REPORTS

of ceramics, shell thickness can be precisely controlled (Fig. 2, B and C). In addition, core-shell colloids whose composition is different on the outside and inside of the hollow shell can be formed (Fig. 2D). Metallic nanospheres and nanoshells are also of interest because of their optical and physical properties (10), yet they are notoriously difficult to prepare in the 50- to 500-nm range by standard chemical methods. We formed them by adapting the metal templating chemistry used to infiltrate opals developed by Yan *et al.* (11). Here, metal oxalate salts that adhere to the polymer walls are reduced by calcination at 450°C for 10 hours. As in the case of the ceramic nanoparticles, hollow colloids are formed that retain the shape of the initial oxalate shells (Fig. 3B).

Many emerging applications for colloidal materials require complex particle morphologies. One form we explored was the hollow colloidal polymer. We chose polypyrrole as a target material because of its possible use in drug delivery applications (12). Successive exposure of a macroporous polystyrene template in a 20% (v/v) pyrrole ethanol solution and a 0.05 M FeCl₃ aqueous solution formed arrays of conductive polypyrrole capsules (Fig. 3A). When the sample is compressed before imaging, the colloids collapse into irregular shapes, much like deflated soccer balls (Fig. 3B). Existing methods for forming

polymer capsules rely on layer-by-layer assembly of polyelectrolytes (13) or the formation of block copolymer assemblies (14), which necessarily limits the choice of polymer materials. In our method, the only constraint placed on the choice of material is that its polymerization must occur under conditions that do not destroy the host template.

The macroporous polymer templates can also be completely filled physically rather than chemically, where they act as a 3D analog of the "soft lithography" elastomeric stamps used to make 2D patterns (15). We have made solid poly(*p*-phenylenevinylene) (PPV) and Au colloidal crystals by filling the macroporous polystyrene films with PPV precursor-methanol solution or gold nanocrystals-hexane solution (16). The solvents were slowly evaporated to deposit solids deep inside the pores, and the templates were removed by dissolution in toluene. The general nature of this physical filling allows one to make solid colloidal crystals from a large number of other materials, including many available nanocrystals.

In most of the prior examples, template filling led to the formation of hollow colloids; it is also possible to form solid colloids using macroporous polymers if the adhesion between the filling phase and the polymer is appropriately controlled. When macroporous polystyrene serves as the host for colloidal

growth, most materials conformally coat the interior polymer void surface during filling (Fig. 1D). In these polymers, colloids grow from the outside in, and after thermal treatment and polymer removal, hollow capsules are the result. A very different process is observed when macroporous poly(methyl methacrylate) (PMMA) is used as a template. Here, the ceramic layer pulls away from the host polymer and forms solid spheres smaller than the cavities (Fig. 1C). Colloidal formation in this instance proceeds from the center outward, and colloids grow successively larger after repeated cycles of immersion and filling. The PMMA template can be burned out using a propane torch in air, leaving an array of solid ceramic spheres (Figs. 1E and 2A). We have found that other inorganic materials (CdS and AgCl) (17) also show a tendency to adhere strongly to polystyrene and not to PMMA. The interfacial free energy between the polymer and ceramic is the main contribution to their apparently different adhesion properties (18). We speculate that the polystyrene functions as a strong π -donating ligand with the metal centers in the inorganic materials, leading to an increased adhesion between the growing colloids and the polystyrene template (19).

In addition to providing for a remarkable range of colloidal materials and architectures, the macroporous polymers are pliable mate-

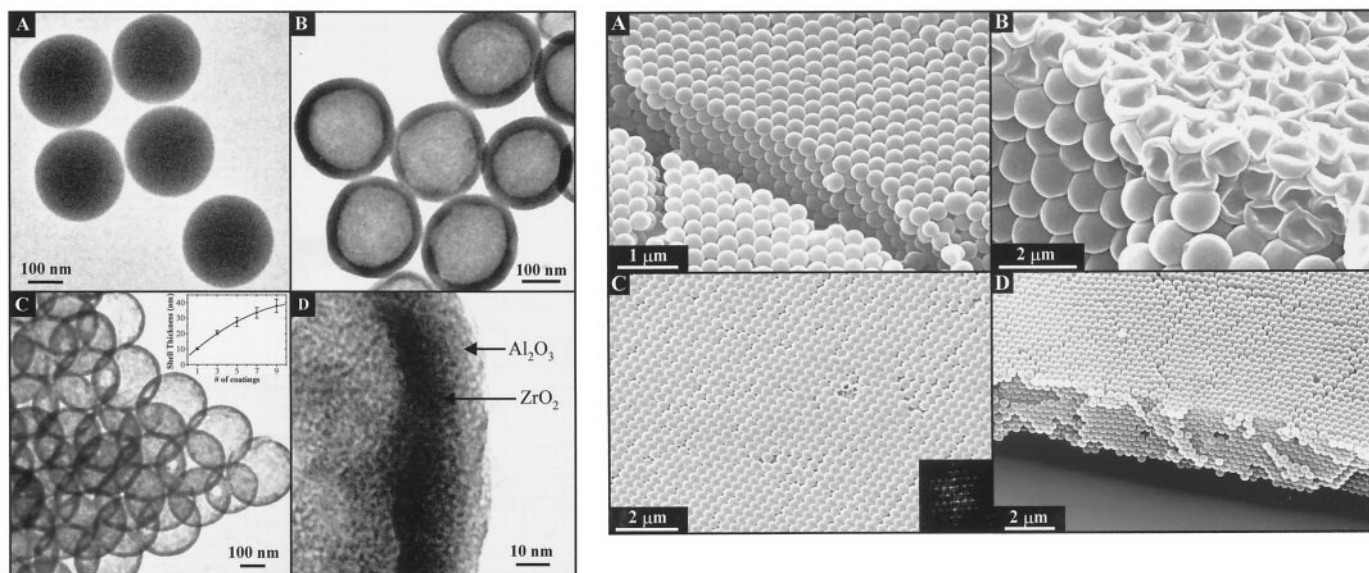


Fig. 2 (left). TEM images of monodisperse particles and colloidal crystals made by the templating method. (A) Solid titania colloids (diameter 262 ± 5 nm) replicated from PMMA template after coating seven times. (B) Hollow titania colloids (diameter 267 ± 14 nm, shell thickness 31.4 ± 2.3 nm) replicated from polystyrene templates after coating seven times. (C) Thinner shell hollow titania colloids (shell thickness 15.4 ± 1.0 nm) replicated from the same template as (B) after coating only twice. The inset shows the relation between shell thickness and number of coatings. (D) Core-shell structure of a hollow zirconia-alumina colloid formed from successive deposition of alumina and then zirconia (each coated twice) on the surface of a polystyrene template. Because zirconia has a higher electron density than alumina, it appears darker in

electron microscopy images. In situ energy-dispersive x-ray (EDX) and microprobe analyses indicate the expected stoichiometric proportions of the materials.

Fig. 3 (right). SEM images of the templated colloidal crystals. (A) The ordered structure of a polypyrrole colloidal crystal replicated from a polystyrene template. (B) The deflated hollow structure of the same sample after being compressed. (C) Top view of a hollow nickel colloidal crystal replicated from a polystyrene template. Several broken colloids are apparent in the image. The inset shows a Fourier transform of a $40 \mu\text{m} \times 40 \mu\text{m}$ region in the (111) plane. In situ EDX analysis indicates that the nickel is relatively pure (>95 atomic %). (D) A solid Al₂O₃ colloidal crystal replicated from PMMA template after coating seven times.

REPORTS

rials that can be compressed or extended to form unusual void shapes. We investigated whether colloids grown in such distorted voids would adopt nonspherical shapes. Nonspherical colloids may offer advantages over their spherical counterparts in applications that require periodic structures with lower symmetries (20). In addition, monodisperse ellipsoidal latex colloids have been introduced as a potential model for rigid rod systems such as liquid crystal polymers and biopolymers (21). Methods for preparing inorganic, polymeric, and metallic colloidal cubes, ellipsoids, and rods have been reported for specific materials (1, 21, 22), but sample

Table 1. Size and size distribution of colloids synthesized by the templating process. More than 200 particles were measured in SEM images to arrive at the values reported. Macroporous polystyrene (PS) samples [void diameter 333 nm (4.3%)] templated from silica colloidal crystals [colloid diameter 336 nm (3.7%)] were used to make all spheres in the middle column; macroporous PMMA samples [void diameter 288 nm (4.8%)] templated from silica colloidal crystals [colloid diameter 294 nm (4.7%)] were used to make all spheres in the right column. N/A, not applicable.

Material	PS template (nm)	PMMA template (nm)
TiO ₂	325.0 (5.2%)	267.8 (4.8%), solid
ZrO ₂	327.1 (5.1%)	271.3 (5.3%), solid
Al ₂ O ₃	327.3 (4.7%)	273.7 (5.5%), solid
Polypyrrole	322.0 (4.8%)	N/A
PPV	310.5 (5.6%)*	N/A
CdS	323.7 (6.3%)	269.6 (6.1%), solid
AgCl	325.2 (5.7%)	270.9 (5.2%), solid
Au	319.7 (5.3%)*	N/A
Ni	306.6 (5.9%)	N/A

*Solid.

homogeneity is poor and a general methodology has not yet been developed.

When a macroporous polymer film is heated above its glass transition temperature (T_g), it becomes a rubber and can be stretched by a uniform uniaxial or biaxial force. The draw ratio D characterizes the magnitude of this extension, and for one-dimensional stretching D is defined as the ratio of the extended length to the starting length. To avoid collapse of the voids during the heating, we fill the pores with mineral oil before heating, which we remove by a heptane wash afterward. If the film is then quickly cooled down below T_g while still constrained in the deformed state, the shape of the stretched voids—oblate for a two-dimensional extension and ellipsoidal for a one-dimensional extension—is fixed into the glassy, inflexible polymer. These nonspherical voids can be replicated into many different materials using the methods described above. The SEM images in Fig. 4, A and B, show top views of two hollow ellipsoidal titania colloidal crystals (23) with different axial ratios, both templated from macroporous polystyrene ($T_g = 94^\circ\text{C}$) (24). The ellipsoidal shapes of the colloids and the long-range order in the (111) plane are confirmed by the elongated hexagonal patterns of the fast Fourier transforms (FFTs) (Fig. 4, A and B, insets). We measured the lengths of the long and short axes of these ellipsoidal colloids made with differing draw ratios ($D_A = 1.3$ and $D_B = 1.7$). The sample in Fig. 4A has a long axis of 489 ± 27 nm, a short axis of 333 ± 18 nm, and an axial ratio of 1.47; the sample in Fig. 4B has a long axis of 624 ± 43 nm, a short axis of 281 ± 14 nm, and an axial ratio of 2.22.

We achieved a high degree of control over the aspect ratio of the resulting col-

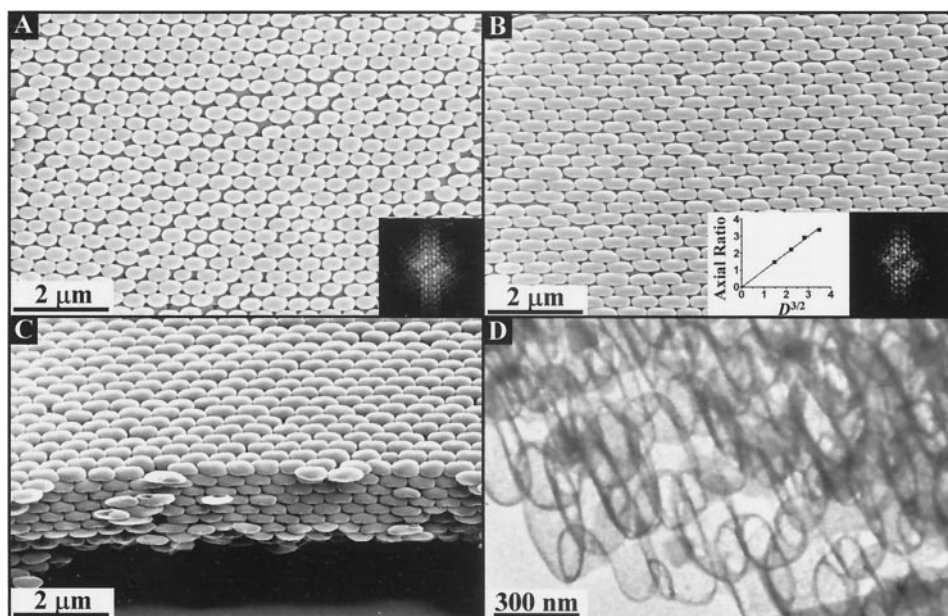
loids. The axial ratios (p) of ellipsoidal samples can be predicted from their corresponding draw ratios (D) by assuming that the volume of the voids does not change during the stretch; this assumption is reasonable because the voids are filled with mineral oil, which is not likely to undergo a large change in density as a result of the modest forces during extension. A brief analysis (25) yields the relation

$$p = b/a = D^{3/2} \quad (1)$$

where b and a are the lengths of the long and short axes of the ellipsoidal colloids, respectively. The measured axial ratios of four ellipsoidal samples with differing draw ratios (Fig. 4B, left inset) agree well with this simple model. A similar result has also been observed in a polystyrene latex-poly(vinyl alcohol) system (21). Axial ratios greater than 5.0 are not feasible because the polymer begins to tear as a result of the tensile force; the use of more flexible polymers such as poly(dimethylsiloxane) (PDMS) may alleviate this problem.

The ordering perpendicular to the close-packed (111) axis of these elliptical colloidal crystals is apparent in the cross-sectional image in Fig. 4C (same sample as Fig. 4B). The sample templated from polystyrene is hollow, as shown by the broken colloids in Fig. 4C and further confirmed by the transmission electron microscopy (TEM) image in Fig. 4D. The ellipsoids are monodisperse with a uniform shell thickness. Thus, heating and stretching does not change the surface properties of the polymer substantially, so all of the morphologies and materials developed for the nonstretched templates can be extended to these nonspherical examples. Because geometric anisotropy has been shown to widen

Fig. 4. Electron microscopy images of ellipsoidal colloidal crystals. (A) Top view of a hollow titania sample (coated four times) templated from a macroporous polystyrene (void diameter 429 ± 16 nm). Draw ratio $D = 1.3$. The inset shows a Fourier transform of a $40 \mu\text{m} \times 40 \mu\text{m}$ region in the (111) plane. (B) Top view of a hollow titania sample (coated four times) templated from the same macroporous polystyrene sample. $D = 1.7$. The left inset shows the linear relation of the axial ratio with $D^{3/2}$. The right inset shows a Fourier transform of a $40 \mu\text{m} \times 40 \mu\text{m}$ region in the (111) plane. (C) Cross-sectional view of the same sample as (B). (D) TEM image of the same sample as (B).



the photonic band gap of colloidal materials (26), ellipsoidal colloidal crystals with a high refractive index may pave the way for building new photonic crystals with superior optical properties.

The primary advantage of this approach to colloidal synthesis is that uniformity control is completely affected by the template, thus transferring this burden to the original silica colloids for which high-quality samples are routinely available. To evaluate how effectively the templating process captured the uniformity of the macroporous voids, we measured the final particle size and size distribution using SEM images such as Fig. 3C. These sizes are compared to the characteristics of the starting silica colloids and macroporous polymer voids in Table 1. Size distributions remained remarkably narrow after the templating steps. The average diameters of colloids templated from PMMA templates show roughly a 10% reduction, which is reasonable given the shrinkage that occurs during the template removal process (27). Although there are chemical methods for producing some of these colloids with relatively narrow size distributions (around 10%) (1, 28), this templating approach provides a strategy for creating a wide range of highly monodisperse colloids (around 5%).

Ultrasonication is a well-established method for breaking up colloidal aggregates in solution (29), and we used it successfully to fragment these colloidal films. Brief treatments (30 s in a 40-W ultrasonic bath) in solvents such as toluene yielded larger pieces of colloidal crystal fragments (several millimeters in size), which were ideal specimens for TEM studies of the array geometry (Fig. 2C). Longer treatments, up to 10 min, provided dispersed material of the type shown in Fig. 2, A and B. These dispersed colloids exhibit uniform surfaces. Although the geometry of the macroporous host contains windows between the spherical voids, colloidal material does not appear to template these channels at an appreciable density. We attribute this to the relative size of the windows, which is only 10 to 20% of the void size, and to the colloidal shrinkage induced during the condensation or polymerization reactions (30).

Except for ultrasonication in appropriate solvents, the templated colloidal crystals are remarkably robust, high-quality materials. The long-range order of the crystals is apparent in SEM images such as Fig. 3C. The FFT of the image provides a measure of order in the (111) plane (Fig. 3C, inset), and it is apparent that the spheres are arranged in a close-packed array (31). Although defects such as cracks and point defects can be observed, the single crystal-

line nature of the starting silica colloidal crystals is retained during the templating process. The ordering perpendicular to the close-packed (111) axis is best visualized in cross-sectional images; Fig. 3D shows an example for an alumina solid sphere sample. These samples are films, not monoliths, and their (111) axis is perpendicular to the underlying glass substrate. The film thickness can be precisely controlled from single monolayers to more than 100 layers because of the faithful replication of the starting silica colloidal crystal (8). Because of their long-range order, these samples have a photonic stop-band comparable to that seen in macroporous titania (27). The spectral position and width of this band for hollow titania colloids depends sensitively on the shell thickness and on the overlap between adjacent spheres (32). Thus, hollow spheres offer another two parameters—shell thickness and aspect ratio—for engineering photonic properties in colloidal systems (26).

References and Notes

1. E. Matijevic, *Langmuir* **10**, 8 (1994).
2. C. J. Brinker, G. W. Scherer, *Sol-Gel Science: The Physics and Chemistry of Sol-Gel Processing* (Academic Press, Boston, 1990); C. B. Murray, D. J. Norris, M. G. Bawendi, *J. Am. Chem. Soc.* **115**, 8706 (1993).
3. P. Pieranski, *Contemp. Phys.* **24**, 25 (1983).
4. A. van Blaaderen, R. Ruel, P. Wiltzius, *Nature* **385**, 321 (1997).
5. F. S. Kleiner, C. J. Mamiya, R. G. Tansey, *Gardner's Art Through the Ages* (Harcourt, Fort Worth, TX, 2000).
6. P. Hoyer, H. Masuda, *J. Mater. Sci. Lett.* **15**, 1228 (1996).
7. S. A. Johnson, P. J. Ollivier, T. E. Mallouk, *Science* **283**, 963 (1999).
8. P. Jiang, J. F. Bertone, K. S. Hwang, V. L. Colvin, *Chem. Mater.* **11**, 2132 (1999).
9. P. Jiang, K. S. Hwang, D. M. Mittleman, J. F. Bertone, V. L. Colvin, *J. Am. Chem. Soc.* **121**, 11630 (1999).
10. S. J. Oldenburg, S. L. Westcott, R. D. Averitt, N. J. Halas, *J. Chem. Phys.* **111**, 4729 (1999).
11. H. Yan *et al.*, *Adv. Mater.* **11**, 1003 (1999). As an example, we started by forming nickel oxalates in polystyrene templates using 0.2 M nickel (II) acetate ethanol/water (v/v: 1/1) solutions as precursors and 1 M oxalic acid ethanolic solutions as precipitating agents. The polystyrene-oxalate composites were then calcined in flowing nitrogen at 450°C for 10 hours. This treatment allowed the polystyrene to be burned out and converted the nickel oxalate into metallic nickel:
$$\text{NiC}_2\text{O}_4 \rightarrow \text{Ni} + 2\text{CO}_2 \quad (2)$$

In the same way, metallic cobalt, copper, cadmium, and lead hollow colloids can also be formed.
12. J. M. Pernaut, J. R. Reynolds, *J. Phys. Chem. B* **17**, 4080 (2000).
13. F. Caruso, R. A. Caruso, H. Möhwald, *Science* **282**, 1111 (1998).
14. J. Ding, G. Liu, *Chem. Mater.* **10**, 537 (1998).
15. E. Kim, Y. Xia, G. M. Whitesides, *Nature* **376**, 581 (1995).
16. The PPV precursor was synthesized as described [V. L. Colvin, M. C. Schlamp, A. P. Alivisatos, *Nature* **370**, 354 (1994)]. After filling, the PPV precursor was converted to conjugated PPV by heating at 80°C under vacuum for 1 hour. The polystyrene template was then dissolved in toluene, and the PPV film was then heated to 350°C under vacuum for 3 hours to form fully conjugated PPV. The gold nanocrystals were synthesized as described [M. Brust, M. Walker, D. Bethell, D. J. Schiffrin, R. Whyman, *J. Chem. Soc. Chem. Commun.* **1994**, 801 (1994)]; 0.2 g of dried gold nanocrystals was dissolved in 10 ml of hexane and used as the filling solution.
17. Aqueous solutions of 0.2 M Cd(NO₃)₂ and AgNO₃, with 20% ethanol by volume, were used as precursor solutions; aqueous solutions of 0.2 M Na₂S and NaCl with the same amount of ethanol were used as precipitating solutions.
18. The overall adhesion energy $E(\text{ad})$ can be expressed as
$$E(\text{ad}) = E(\text{polymer}) + E(\text{ceramic}) - \gamma(\text{polymer-ceramic}) \quad (3)$$

where $E(\text{polymer})$ and $E(\text{ceramic})$ are the surface free energies for polymer and ceramic, respectively, and $\gamma(\text{polymer-ceramic})$ is the interfacial free energy (19). Because PMMA and polystyrene have similar surface free energies (24), and because for the same ceramic $E(\text{ceramic})$ is the same, the difference between the two polymers must lie in the interfacial free energy.
19. F. Garbassi, M. Morra, E. Occhiello, *Polymer Surfaces: From Physics to Technology* (Wiley, Chichester, UK, 1998).
20. Y. Xia, B. Gates, Y. Yin, Y. Lu, *Adv. Mater.* **12**, 693 (2000).
21. M. Nagy, A. Keller, *Polym. Commun.* **30**, 130 (1989).
22. C. C. Ho, R. H. Ottewill, L. Yu, *Langmuir* **13**, 1925 (1997).
23. Macroporous polystyrene strips (4 by 1 by 0.4 cm) were clamped into a metal frame and filled with mineral oil, then stretched to a length corresponding to a preset draw ratio in an oven preheated to 110°C. The metal frame used is similar to the one described [C. C. Ho, A. Keller, J. A. Odell, R. H. Ottewill, *Colloid Polym. Sci.* **271**, 469 (1993)]. The total heating time in the oven was about 2 min. The quickly cooled strips were then washed by heptane three times and used as templates for hollow titania, as before. For an illustration of the frame and a further description of the process, see *Science Online* (www.sciencemag.org/cgi/content/full/291/5503/453/DC1).
24. J. E. Mark, *Physical Properties of Polymers Handbook* (AIP Press, Woodbury, NY, 1996).
25. The ellipse major and minor axes are related to the starting sphere diameter by
$$4/3 \times \pi r^3 = 4/3 \times a^2 \times b \quad (4)$$

where r is the radius of the spherical voids, and a and b are the semi-axes of the ellipsoidal voids. In addition, the long semi-axis can be related to the draw ratio by
$$b = D \times r \quad (5)$$

where D is the draw ratio. Substitution of Eq. 5 into Eq. 4 yields $a = D^{-1/2} \times r$. Thus, the axial ratio $\rho = b/a = D^{3/2}$ (Eq. 1).
26. Z. Li, L. Lin, B. Gu, G. Yang, *Physica B* **279**, 159 (2000).
27. B. T. Holland, C. F. Blanford, A. Stein, *Science* **281**, 538 (1998); J. E. G. Wijnhoven, W. L. Vos, *Science* **281**, 802 (1998); O. D. Velev, T. A. Jede, R. F. Lobo, A. M. Lenhoff, *Nature* **389**, 447 (1997).
28. T. Sugimoto, *Adv. Colloid Interface Sci.* **28**, 65 (1987).
29. Z. Zhong, Y. Yin, B. Gates, Y. Xia, *Adv. Mater.* **12**, 206 (2000).
30. A. Imhof, D. J. Pine, *Nature* **389**, 948 (1997).
31. In addition, we can directly observe the relative positions of the crystallization planes from TEM images of hollow-sphere colloidal crystals (Fig. 2C) by consecutively focusing on stacked crystallization planes. We found in several images of four to six layers that the spheres are stacked in an ABCABC pattern consistent with a face-centered cubic (fcc) structure. Although such microscopic evidence is not an accurate measure of the average stacking in an entire crystal, we note that the fcc packing is expected to be more stable than hexagonal close-packing (hcp), even for hard spheres [L. V. Woodcock, *Nature* **385**, 141 (1997)].
32. R. Rengarajan, P. Jiang, V. L. Colvin, D. M. Mittleman, *Appl. Phys. Lett.* **77**, 3517 (2000).
33. Supported by NSF (grant CHE-9702520) and the Welch Foundation (grant C-1342). We thank D. M. Mittleman for many useful discussions.